

# Towards Reliable Image Outpainting: Learning Structure-Aware Multimodal Fusion with Depth Guidance

Lei Zhang, Kang Liao, Chunyu Lin\*, Yao Zhao  
Institute of Information Science, Beijing Jiaotong University  
Beijing, China

## ABSTRACT

Image outpainting technology generates visually reasonable content regardless of authenticity, making it unreliable to serve for practical applications even though introducing additional modalities *eg.* the sketch. Since sparse depth maps are widely captured in robotics and autonomous systems, together with RGB images, we combine the sparse depth in the image outpainting task to provide more reliable performance. Concretely, we propose a Depth-Guided Outpainting Network (DGONet) to model the feature representations of different modalities differentially and learn the structure-aware cross-modal fusion. To this end, two components are designed to implement: 1) The *Multimodal Learning Module* produces unique depth and RGB feature representations from the perspectives of different modal characteristics. 2) The *Depth Guidance Fusion Module* leverages the complete depth modality to guide the establishment of RGB contents by progressive multimodal feature fusion. Furthermore, we specially design an additional constraint strategy consisting of *Cross-modal Loss* and *Edge Loss* to enhance ambiguous contours and expedite reliable content generation. Extensive experiments on KITTI demonstrate our superiority over the state-of-the-art methods with more reliable content generation.

## CCS CONCEPTS

• **Computing methodologies** → **Image processing**; *Computer vision representations*.

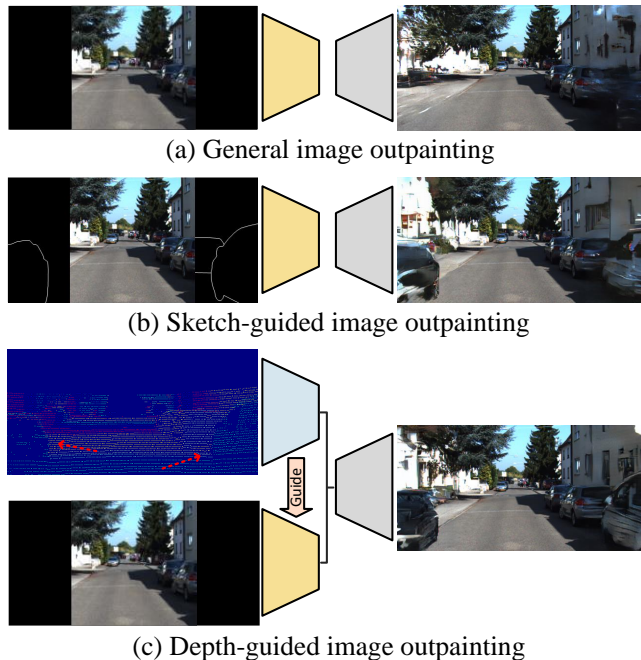
## KEYWORDS

Image Outpainting, Depth Perception, Multimodal Fusion, Generative Model

## 1 INTRODUCTION

Image outpainting aims to extrapolate the unknown image content, generating reasonable contents based on the style and structure. Previous related research could be approximately divided into two categories: traditional completion algorithms [15, 23, 29, 41] and learning-based solutions [7, 16, 26, 30, 34, 38, 40]. In particular, inspired by the generative adversarial networks (GANs), the learning-based methods make the outpainting results more accurate and believable [19, 20] like Fig1(a). In the recent studies, researchers [4, 12, 13, 38] propose to introduce additional modal information to the general image outpainting tasks. For instance, the sketch of unknown areas was introduced [31] to encourage the filled regions to produce sketch-like content, as shown in Fig1(b). These works focus on blending various modal contents to reach better outpainting performance for their target scenes.

However, the extrapolated results generated by the existing methods are conjectures in terms of the inference preference learned



**Figure 1: A comparison of different image outpainting tasks: (a) general image outpainting, (b) sketch-guided image outpainting, and (c) the proposed depth-guided image outpainting.**

from the training samples. They drive the network to fantasize: what the content might look like outside the boundaries? So the generated extrapolation is fictitious, even if the model could show a visually reasonable appearance. It cannot reflect the reality outside the image. Therefore, to enable the network the capability to infer credible and realistic scenes, we propose to introduce an additional modality that could reflect the real surroundings to make the outpainting contents reliable. To this end, the sparse depth converted from LiDAR point clouds could be a satisfying selection because it can reflect the structure of the objects and the distribution of scenes naturally. Besides, it has a broader field of view than the camera image, making it reasonable for the depth to guide the reliable outpainting. Furthermore, it has been widely used in multimodal works [11, 33] related to robotics and autonomous driving system, showing new vigor and potential vitality for outpainting to serve practical multimodal applications. In this work, we propose to employ the sparse depth modality of the surroundings to assist the image outpainting of RGB images like Fig1(c). Since there is a non-negligible cross-modal discrepancy between the sparse depth map

and the RGB image, our main challenge is how to extract beneficial assistance from the depth modality and combine it with the RGB modality to facilitate reliable and realistic outpainting results.

To achieve this goal, we propose the Depth-Guided Outpainting Network (DGONet) to learn the structure-aware multimodal fusion with sparse depth, which generates the extrapolated images embodying the actual environment. The sparse depth and RGB have two major modal differences: 1) the pixel values carry different messages – depth and intensity; 2) the valid pixels in the depth map from LiDAR are significantly sparser than that in the RGB image. Thus we design a *Multimodal Learning Module* to extract unique feature representations from different modalities, contributing to more beneficial and discriminative semantic representations from their low-level features. When it comes to multimodal feature fusion, the previous works[10, 18] roughly adopt the concatenation operation in channels to implement the interaction between the two modal features. They omit the respectively modal roles in different tasks, and the interaction is pretty weak. To improve it, we design a *Depth Guidance Fusion Module* to encourage the depth modality to facilitate the establishment process of extrapolated RGB contents. Particularly, this module adopts a progressive fusion scheme to enhance feature interaction by converting the depth features into discriminative convolutional kernels to filter the RGB features, generating semantic-consistent fused features with the depth features.

Considering the significant content loss in RGB images, we propose a *Cross-modal Loss* to spread the valid feature of the depth to the unknown region of the RGB feature directly. It forces the extrapolated RGB feature to be similar to the high-level semantics of the depth modality, assisting the reconstruction of authentic content consistent with depth. To avoid the boundary-blurring phenomenon occurring continually in generating tasks, we introduce an *Edge Loss* to constrain the model to generate sharp object outlines in the results. In addition to the three commonly used metrics for image generation, we design a vehicle detection metric to measure the network’s performance on the reliability to reflect the consistency with the real surroundings. To sum up, our contributions can be summarized as follows:

- We establish a new reliable image outpainting task combining sparse depth to reach the realistic extrapolation, where a Depth-Guided Image Outpainting network is presented to accomplish the structure-aware multimodal fusion.
- We design a *Multimodal Learning Module* to learn the modality representation difference with sparse depth and RGB, and a *Depth Guidance Fusion Module* to guide the generation of extrapolation by fusing multimodal features progressively. Besides, *Cross-modal* and *Edge Loss* are designed to enhance the reliability of the results further.
- We propose the average precision of vehicle detection as an objective measure for the authenticity of extrapolated results. Experimental results demonstrate our superiority in popular outpainting metrics and reliability compared with the state-of-the-art methods on the KITTI[27] dataset.

## 2 RELATED WORK

**Image Inpainting** The goal of image inpainting is to paint the defective areas inside the image to make the image complete and reliable. The original image inpainting studies were based on the traditional methods[1–3], which borrowed the regular texture or patch synthesis of the surrounding area. These methods work well for static textures but are limited to non-static data such as human faces or natural scenes. After the rise of deep learning-based adversarial generative networks[21, 35, 36, 36], it has extensive efforts dedicated to this field. Xie *et al.*[32] introduced a learnable attention map for feature re-normalization to allow the model to focus on filling irregular holes effectively. Yu *et al.*[37] proposed to use a free-form mask based on the learnable gated convolution guidance to generate higher-quality results. These methods were widely used as basic backbone networks in state-of-the-art research.

**Image Outpainting** The traditional image outpainting methods [29, 41] searched input-related relevant patches from the pre-defined candidate pool to stitch with input. So they are not precise enough and hard to apply to other complex scenes. Driven by deep learning and GAN, the image outpainting methods based on neural network [12, 30] also had a more authentic performance. Teterwak *et al.*[7, 7, 26, 34] introduced semantic conditions to GAN’s discriminator to obtain coherent texture and semantic representation. In particular, more recently, the focus of image outpainting research has shifted to introducing additional information to guide synthesis [38] Khurana *et al.*[12] realized an image outpainting based on the result of semantic segmented image, then extrapolated and eventually painted the texture to these semantics. Wang *et al.*[31] proposed the use of the Holistic Alignment Module and Sketch Alignment Module, which respectively focused on the whole and details, to achieve the image outpainting by introducing sketch information. Bowen *et al.*[4] introduced the mask of the foreground object to obtain more robust extrapolation results. They factored out the object explicitly and predicted object mask and texture, respectively. However, existing methods were only focused on generating visually pleasant images but provided no authenticity for the final synthesis. Therefore, the previous would produce plausible but unrealistic results.

## 3 METHODS

Our goal is to synthesize the additional contents on both sides of the restricted RGB assisted by sparse depth. We provide an overview of the overall architecture in Fig.2, in which the DGONet consists of a generator  $G$  and a conditional discriminator  $D$ .

### 3.1 Multimodal Learning Module

Since our inputs consist of two modalities whose representations are different, we design the *Multimodal Learning Module* to capture unique characteristics respectively.

**3.1.1 Depth-domain Branch.** In this branch, we take a single channel sparse depth map as input. On the one hand, compared with RGB images, depth maps have little complex texture information and intuitively describe the surroundings and positions of the salient objects. It is beneficial to guarantee authentic extrapolation. On the other hand, it has an obvious disadvantage that the depth

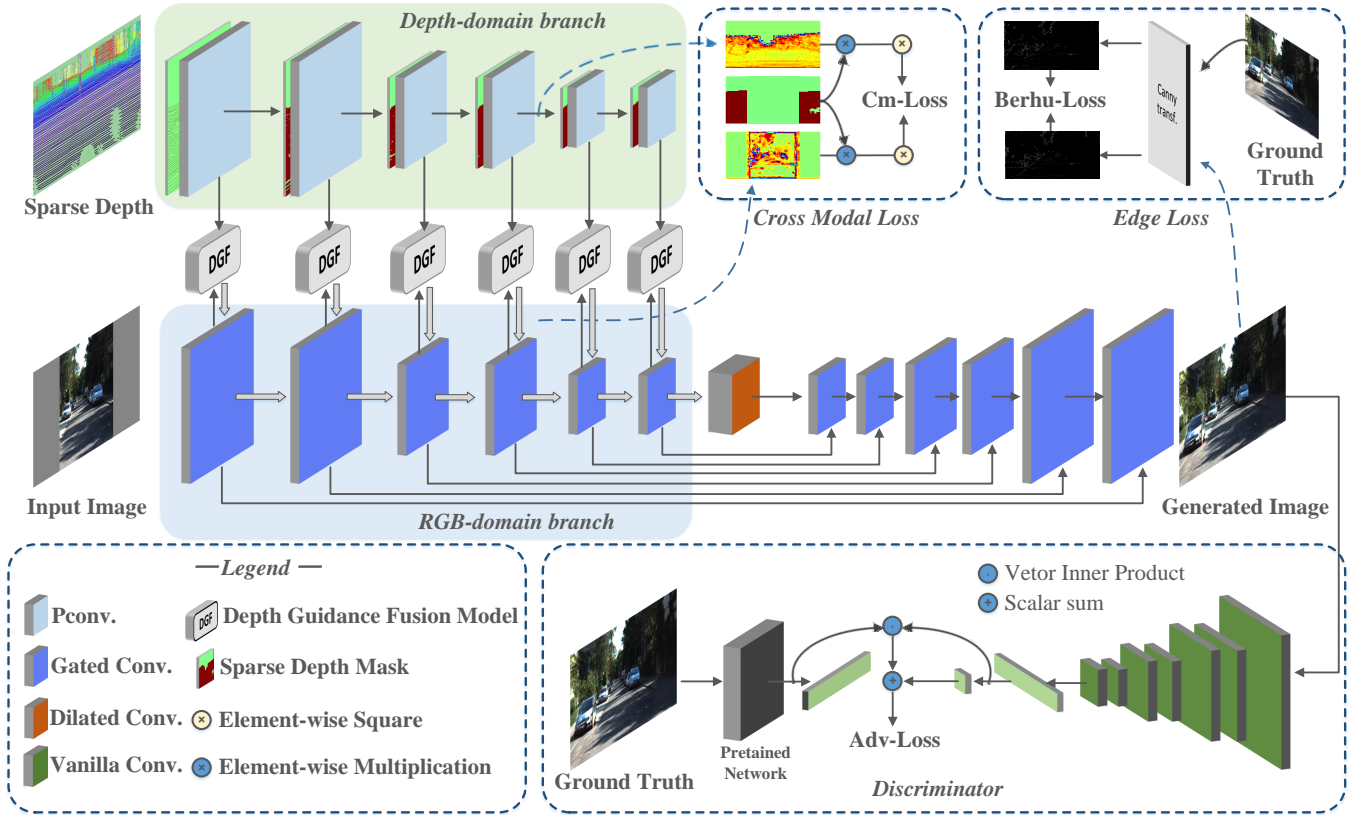


Figure 2: An overview of the network architecture

maps mapped from LiDARs are extremely sparse in pixels, which has only 7% **valid pixels**[27] on the whole data distribution. As a result, the general convolution networks that treat all pixels equally can be perturbed by a large proportion of invalid pixels severely like the second row of Fig3. To address this problem, we build a Depth-domain branch in which each layer uses partial convolution[17] to enable the model to overcome the impact of sparseness. Specifically, we set the valid pixels of the sparse depth to 1 and the invalid ones to 0 to form a sparse depth mask  $M_{SD}$ . The depth features are multiplied with  $M_{SD}$  before each layer, which assures the output is only affected by the convolution of valid pixels. In other words, the adverse effects of invalid pixels would be eliminated entirely. The detailed implementation of the branch is formulated as follows:

$$F_D^{n+1} = \text{Conv}(F_D^n \odot M_{SD}^n) \frac{\text{sum}(I)}{\text{sum}(M_{SD}^{n+1})} \quad (1)$$

where  $\odot$  denotes the element-wise multiplication.  $F_D^n$  represents the feature of the  $n$ -th layer in the Depth-domain branch.  $I$  is an all-one matrix that has the same shape as  $M_{SD}$ . In this way, we count the proportion of valid pixels in the  $M_{SD}$  as the scaling factor, which is applied as an appropriate normalization operation for the convolution, adapting to the varying amount of valid inputs and reducing the impact of sparsity. Besides, the  $M_{SD}$  is also updated by the convolution operation at each layer (assuming the kernel

size is 3):

$$\Omega = \begin{bmatrix} 1 & 1 & 1 \\ 1 & 1 & 1 \\ 1 & 1 & 1 \end{bmatrix}, \quad (2)$$

$$M_{SD}^{n+1} = \text{Conv}(M_{SD}^n; \Omega)$$

where  $\text{Conv}(\cdot; \cdot)$  denotes the convolution operation. It guarantees that  $M_{SD}$  updates are based on valid pixels. The updates would also be implemented along with the encoding process. The  $M_{SD}$  has an extra effect on the loss computation of our task. In this branch, each layer is followed by an instance normalization layer[28] and ELU activation[6].

**3.1.2 RGB-domain Branch.** In this branch, the input is a color image with blank regions on both sides. Similarly, we set up a binary mask where the valid pixel is set to 1, and the others are set to 0 as an alpha mask  $M_\alpha$ . We concatenate  $M_\alpha$  with the three-channel RGB image and feed them into this branch. As in [26, 37], the gated convolution[37] is employed to form RGB-domain Branch for extracting RGB features, which enables the model to learn a dynamic feature selection mechanism for each channel and spatial location for better filling holes. We establish the forward pass of the RGB-domain branch as Eq.3

$$F_R^{n+1} = \delta(\text{GatedConv}(F_R^n, F_D^{n+1}, M_\alpha)) \quad (3)$$

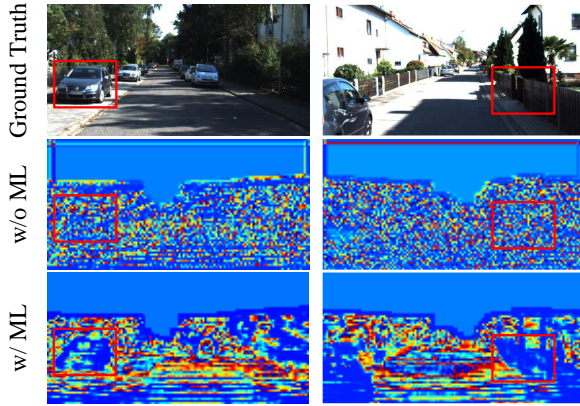


**Figure 3: Feature visualization of the last layer in the Depth-domain Branch. ML indicates the *Multimodal Learning Module*.**

where  $F_R^n$  represents the RGB feature of the  $n$ -th layer, and  $\delta(\cdot)$  represents our *Depth Guidance Fusion Module*. We merge the features into the decoder through skip connections[22], thereby improving the ability of the model to synthesize high-frequency information. To maintain consistency with the Depth-dominant branch, we also employ the instance normalization layer and ELU activation and set the identical feature size and number of channels in the corresponding layer.

### 3.2 Depth Guidance Fusion Module

In the encoding stage, we learn the representation of each modality through analyzing the characterization of the two modalities and establishing branches differently. Then, during the feature fusion, the concatenation between the two modalities was widely used in existing multimodal tasks[10]. But these methods only perform common feature merging to achieve the modal interaction while ignoring the respective roles of modalities in different tasks. Therefore, in our task, we reconsider the role of depth for RGB and design the *Depth Guidance Fusion Module* to restore the authentic RGB content with the guidance of global depth structure, which performs a progressive fusion of the two modalities and utilizes the depth map to guide the generation of RGB as shown in Fig4.

We take the depth feature  $F_D$  and the RGB feature  $F_R$  of the identical layer as the inputs of the module. A  $1 \times 1$  convolutional layer is leveraged as a preliminary basis for the feature integration of the two modalities. Then we use  $M_\alpha$  as an additional channel of the feature, which provides a significant advantage that emphasizes the network to pay attention to the content generation in the blank mask positions. Another  $1 \times 1$  convolutional layer introduces  $F_R$  as the residuals and compresses the number of channels to be consistent with  $F_D$ . The above implementation is shown in the Eq.4:

$$F'_R = \text{conv}_1(\text{conv}_3(\text{conv}_1(F_R \oplus F_D) \oplus M_\alpha) \oplus F_D) \quad (4)$$

where  $\oplus$  denotes the concatenation operation along the channel dimension.  $\text{conv}_1$  and  $\text{conv}_3$  represent the kernel sizes are  $1 \times 1$  and  $3 \times 3$  respectively. Further, inspired by the guided image filtering[8]

and guided convolution[25], we generate the filtering kernels from depth feature  $F_D$  which has the intact content and object distribution structure. Subsequently, the kernel weight  $W_D$  is directly learned from the Kernel-Generating Layer, which is implemented by convolution for grid images. We apply it to the feature  $F'_R$  generated by the modality fusion, which is formalized explicitly as follows:

$$F_{\text{output}} = \text{Conv}(F'_R; W_D(F_D; \Theta)) \quad (5)$$

where  $\Theta$  is the parameter of the Kernel-Generating Layer.

By these implementations, the kernel generated from the depth modality is dynamically transformed depending on the content, thus different kernels would be generated in different depth inputs. And when the incomplete RGB image is fed into the model, the corresponding kernels are applied to related spatial positions. These advantages are suitable for our image outpainting goals. As a benefit of the well-structured depth features, the correct filter is learned at each scene and spatial position. Therefore, we could employ the depth kernel in the unknown area to build the structure-aware RGB content at the corresponding spatial position.

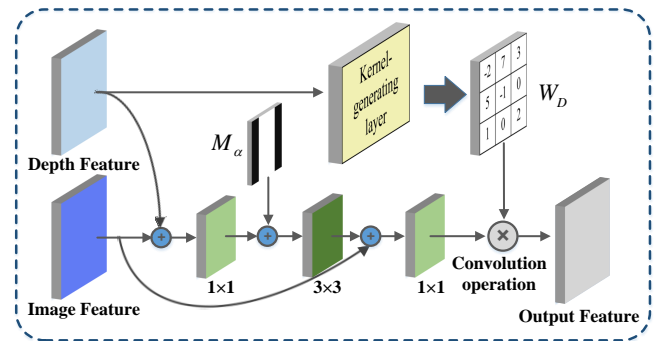


**Figure 4: Implementation of *Depth Guidance Fusion Module*.**

### 3.3 Training Loss

**3.3.1 Cross-Modal Loss.** In the image outpainting, the RGB inputs are incomplete and have larger vacancies than other image completion tasks. Thus, the encoder cannot generate intact contents with the convolution network perfectly, which results in the learned features being barren within extrapolation areas, even remaining a few invalid pixels. While we expect to establish valid contents as quickly as possible during the forward passing in analogy to the manual painting process requiring enough pigment. If the RGB features acquire more structurally comprehensive contents in the encoder stage, the decoder will perform better during the scene reconstruction. In consequence, we design the *Cross-modal Loss* between the features of the fourth layer in the *Multimodal Learning Module* of different modal domains, as formulated:

$$\phi(F) = \frac{1}{M} \sum_i (F^i \odot F^i) \quad (6)$$

$\mathcal{L}_{cm} = \|\phi(F_D \odot (1 - M_\alpha)) - \phi(F_R \odot M_{SD} \odot (1 - M_\alpha))\|_{l_2}$  where  $F^i$  represents the  $i$ -th channel of feature  $F$  and  $M$  represents the number of channels. We element-wise square the pixels of each channel, then accumulate and average them in the channel

dimension. And we utilize  $M_{SD}$  generated from the Depth-domain branch and  $M_\alpha$  to implement constraints only in the extrapolation areas. Finally, the constraint is calculated by L2 loss together with the two-modal feature processing results. Through the constraint, the unbroken depth modality transfers proper features to the RGB modality, assisting the representation of unknown regions to be more robust and providing more pigments for subsequent layers.

**3.3.2 Edge Loss.** Generally, the generated results from decoder reconstruction are blurred since restoring high-frequency information is deficient, especially overlapping between objects and backgrounds. Therefore, we design to set constraints on the edge between the outline of the foreground object and the background to eliminate the blurring of generated results. In the implementation, the edge map is constrained by Berhu loss[42] as shown in the Eq.8:

$$Berhu(x, y) = \begin{cases} \delta |x - y| - \frac{1}{2}\delta^2 & \text{for } |x - y| \leq \delta \\ \frac{1}{2}(x - y)^2 & \text{otherwise} \end{cases} \quad (7)$$

$$\mathcal{L}_{edge} = Berhu(f_{canny}(I_{output}), f_{canny}(I_{GT})) \quad (8)$$

where  $\delta$  is the threshold of Berhu loss, which is set to 0.2 by default. We feed the output with the ground truth into the filter to calculate the edge maps. Thus we manually implement the canny[5] filter so that the edge map could be back-propagated in training.

**3.3.3 Discriminative Loss.** Our DGONet includes a discriminator for the adversarial learning, as shown in Fig2, which judges whether the generator results are a plausible extension of the inputs. Concretely, the generated images are overwritten in known areas by generator inputs and concatenate with  $M_\alpha$  together as discriminator inputs. In addition, we introduce a pre-trained network (InceptionV3[24]) to obtain a learned conditional vector on the input like [26]. It takes an inner product with the discriminator output vector to form the final discriminant result, as shown in Fig.2, which emphasizes that the generated results semantically match the ground truth, especially to prevent semantic drift in extended regions that are farther from the known. In adversarial loss, we use a Wasserstein GAN hinge loss[19]:

$$\begin{aligned} \mathcal{L}_{adv,D} &= E_{I_{GT} \sim P_\chi(I_{GT})} [\text{ReLU}(1 - D(I_{GT})) + \text{ReLU}(1 + D(I_{output}))] \\ \mathcal{L}_{adv,G} &= E_{I_{GT} \sim P_\chi(I_{GT})} [-D(I_{output})] \end{aligned} \quad (9)$$

where ReLU is the rectified linear unit function.

In addition to the loss strategy designed above, we also introduce a pixel loss to optimize for the coarse image agreement, and is implemented as an L1 loss as Eq.10:

$$\mathcal{L}_{pixel} = \|I_{output} - I_{GT}\|_{L1} \quad (10)$$

The total loss of our framework can be described as:

$$\mathcal{L}_{total} = \lambda_{adv}\mathcal{L}_{adv,G} + \lambda_p\mathcal{L}_{pixel} + \lambda_e\mathcal{L}_{edge} + \lambda_{cm}\mathcal{L}_{cm} \quad (11)$$

where  $\lambda_{adv}$ ,  $\lambda_{edge}$  and  $\lambda_{cm}$  are the trade-off factor weights.

## 4 EXPERIMENTAL RESULTS

### 4.1 Experiment Setup

**4.1.1 Datasets.** We train DGONet on the KITTI dataset[27] which were collected on the streets in life and contained corresponding sparse depth maps. In the implementation, we set the known area size to  $256 \times 256$ , respectively expanding the range of  $256 \times 128$  in

the left and right directions of the known area, meaning that each side extrapolates by 50%. Thus the size of the input and output is  $512 \times 256$  identically. We acquire the training data by center-cropping with the KITTI to  $512 \times 256$  about both modalities. Comprehensively considering the dataset sampling frequency and the number of training data, we extract a quarter of the KITTI dataset at equal intervals as training data. It covers more scenes with a small amount of data to enhance the generalizability of the model. In total, we employ 8912 images as training data, and the rest 958 images are taken as testing data.

**4.1.2 Implement Details.** Our network is implemented by the PyTorch platform and trained on an NVIDIA GTX 2080ti GPU. The parameters of the generator and discriminators are jointly updated using the Adam optimizer[14] with batch size 4. The weight  $\lambda_p$  and  $\lambda_{adv}$  are set to 1.0 and 0.01, and  $\lambda_{cm}$  and  $\lambda_e$  are fixed to 1.0 and 5.0. The training first iterates to 100 epochs by only using  $\mathcal{L}_{pixel}$  and  $\mathcal{L}_{adv,G}$ . After this warm-up stage, we further add  $\mathcal{L}_{cm}$  and  $\mathcal{L}_{edge}$  to supervise our network. The gradual benefits of different loss terms are described in the Ablation Study part.

**4.1.3 Evaluation Metric.** We adopt four metrics in the image outpainting task to evaluate the proposed method quantitatively. They contain three commonly standard image evaluation *i.e.* the Fréchet Inception Distance(FID)[9], the Learned Perceptual Image Patch Similarity(LPIPS)[39] and The Peak Signal to Noise Ratio(PSNR). In the generation task, many factors would affect human perception, so the learn-based perception similarity measures such as LPIPS and FID score are more consistent with human perception. Furthermore, considering our motivation is to enable outpainting images the capability to infer realistic scenes, we introduce the average precision (AP) of object detection, which is obtained by detecting vehicles in the outpainting images, to objectively reflect the credibility of the outpainting and the performance of restoration.

### 4.2 Quantitative Evaluations

Table3 shows the results of our method and the state-of-the-art image outpainting methods in the street scene of KITTI datasets. The comparison methods included Boundless[7], Outpainting-SRN[30], and spiralNet[7], which are retrained by the same dataset. It can be observed that our method outperforms all compared methods on four metrics, especially the FID of our approach can reach 25.52, which has a nearly 10 improvement over others. A lower FID represents a closer distribution distance between generated results and ground truth and a higher quality of generated images. In the widely used measure of picture quality, PSNR, the minimum gain reaches 1.02 among the DGONet and others. Our method also performs better on LPIPS, which has the 11.9% percentage gain, indicating our results are more consistent with human perception. In terms of authenticity, the AP is increased from 68.13% to 79.23%, with an improvement of 11.1%, which surpasses the comparison methods by a large margin, verifying the reliability of our proposed.

### 4.3 Qualitative Comparisons

To intuitively demonstrate the credible performance of the proposed, we provide qualitative comparison results in Fig 5. We zoom



Figure 5: Qualitative results with the state-of-the-art methods



Figure 6: Qualitative results on vehicle detection

in on the noteworthy extrapolation areas and mark them with a dotted box. The first row shows the RGB input images of the network. On its right side, we also exhibit the sparse depth representation corresponding to the dotted box. As we can see in this figure, the Outpainting-SRN[30] cannot reconstruct the approximate shape of the objects at the edge position. As for the Boundless[26] and SpiralNet[7], although they can generate partially similar shapes and contents of the objects at the boundary, with further distances and unknown structural layouts, there would be more confusing contents. Instead, our method accurately continues the style and

content of the image at the boundary. It establishes appropriate structures at a further distance based on the features learned from cross-modal fusion. For the colored depth map and enlarged results, our method structurally restores the spatial hierarchy represented by depth modalities, like vehicles, trees, flagpoles, buildings, and ground backgrounds.

In addition, Fig6 shows the comparison of vehicle detection results of the four methods. In the first column, we splice the color pixels of the known region with the sparse depth of the unknown region for visual display. In the second to fourth columns,

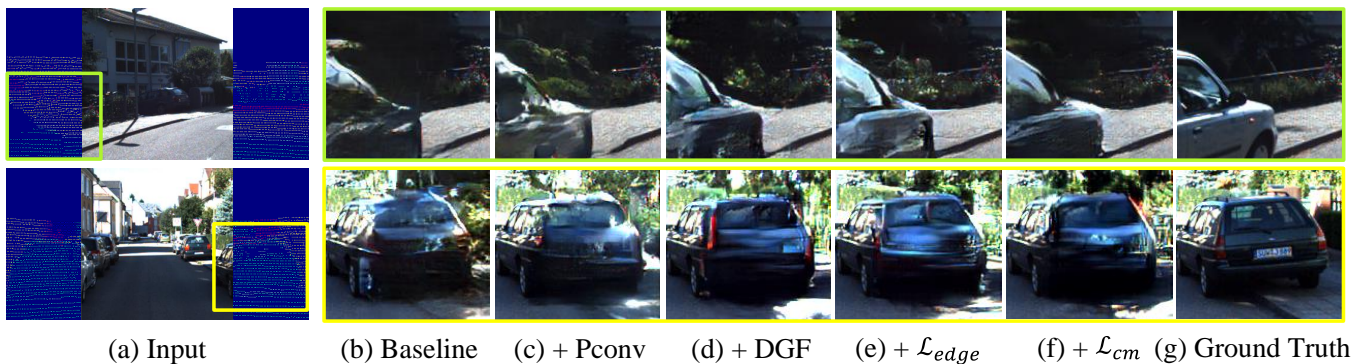


Figure 7: Ablation experiments accumulate component by component. From left to right, the modules are subsequently stacked to synthesize the results.

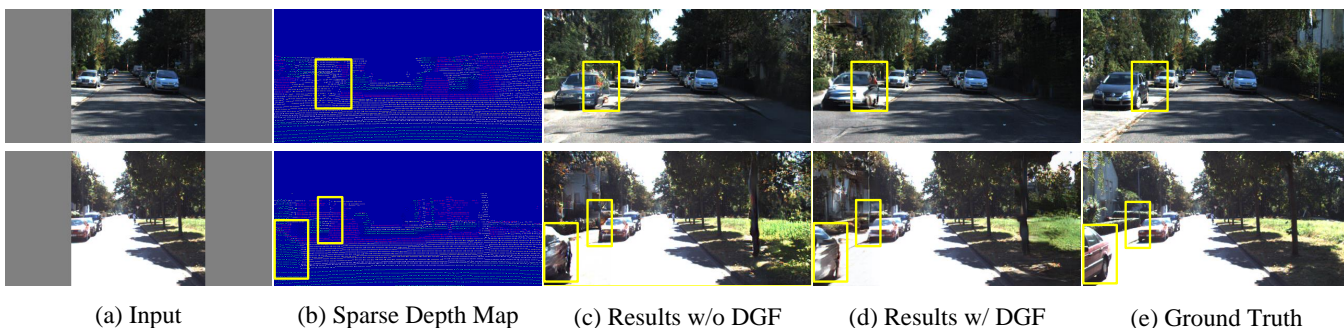


Figure 8: Ablation experiments on *Depth Guidance Fusion Module*.

Table 1: Quantitative comparison results in terms of FID(the lower the better), AP(the higher the better), PSNR(the lower the better) and LPIPS(the lower the better) score with three state-of-the-art general image outpainting methods.

Methods	FID↓	AP ↑	PSNR ↑	LPIPS↓
SpiralNet[7]	45.56	66.72%	15.02	0.2553
Outpainting-Srn[30]	34.99	68.13%	15.25	0.2477
Boundless[26]	32.13	67.96%	15.13	0.2544
Ours	<b>25.52</b>	<b>79.23%</b>	<b>16.27</b>	<b>0.2182</b>

Table 2: The contribution of each part. ML, DGF,  $\mathcal{L}_{edge}$  and  $\mathcal{L}_{cm}$  indicate *Multimodal Learning Module*, *Depth Guidance Fusion Module*, *Edge Loss* and *Cross-modal Loss*, respectively.

	ML	DGF	$\mathcal{L}_{edge}$	$\mathcal{L}_{cm}$	FID↓	AP ↑	PSNR ↑	LPIPS↓
Baseline	✗	✗	✗	✗	29.21	76.95%	15.85	0.2313
Baseline	✓	✓	✓	✗	25.55	79.19%	16.03	0.2215
Baseline	✗	✓	✓	✓	25.64	78.70%	16.11	0.2213
Baseline	✓	✗	✓	✓	25.89	78.30%	15.97	0.2212
Baseline	✓	✓	✓	✓	<b>25.52</b>	<b>79.23%</b>	<b>16.27</b>	<b>0.2182</b>

some defective cars located at the boundary or completely beyond

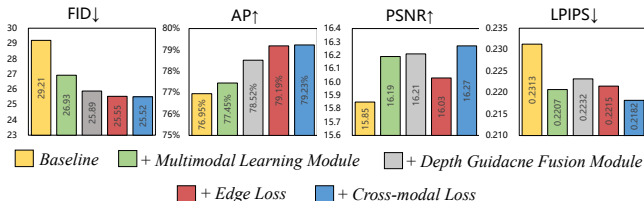


Figure 9: Ablation experiments on four metrics. The modules are accumulated one by one from left to right in the histogram.

the boundary are detected incorrectly or unrecognizable, and misidentification would occur in the chaotic poor-performing areas. While the vehicles established by our method have incredible performance in human perception and object recognition due to their perfect contour structure and correct semantic manifestation.

#### 4.4 Ablation Studies

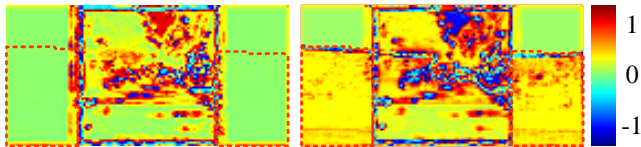
To verify the effectiveness of components in our DGONet, we conduct ablation experiments on the proposed modules, the results are shown in Table 3 and Fig9. Our baseline only employs the vanilla convolution and the gated convolution as the basic network, which utilizes the concatenation operation on the fusion of two modal features. The total loss function is composed of adversarial loss and

pixel loss. From Table3, the model achieves the best results on four metrics when all components are utilized simultaneously. And Fig 7 shows the visual ablation of interesting regions of one example, to intuitively verify the contribution of each component.

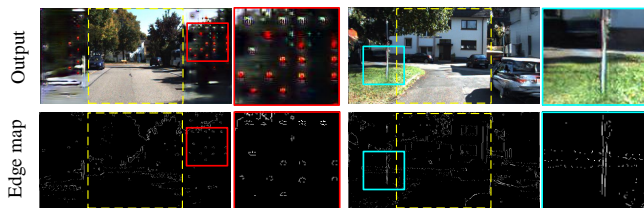
**Table 3: Ablation experiments on the Cross-modal Loss.**

	FID↓	AP ↑	PSNR ↑	LPIPS↓
w/o $\mathcal{L}_{cm}$	25.55	79.19%	16.03	0.2215
$\mathcal{L}_{cm}@Conv4$	<b>25.52</b>	<b>79.23%</b>	<b>16.27</b>	<b>0.2182</b>
$\mathcal{L}_{cm}@Conv6$	25.55	78.68%	16.24	0.2191

**4.4.1 Effectiveness of the Multimodal Learning Module.** First, we add the *Multimodal Learning Module* based on the Baseline to verify its role as a comparison of ablation, and the results are shown in the second row of Table3. Meanwhile, both feature maps of the depth-domain branches are visualized respectively in the comparison, as shown in Fig3. The Baseline of the first row results in cluttered features representation caused by invalid pixels due to sparsity. It also weakens the effect of the depth-domain branch. Through the special design of sparsity depth modality, our ML module can better deal with the problem and obtain the concrete depth feature during encoding. This is also shown in the second line of Fig3, the results express more consistent with the content distribution of the original image. Therefore, the performance in the perception evaluation score has been greatly improved in Table3.



(a) Feature w/o *Cross-modal Loss* (b) Feature w/ *Cross-modal Loss*  
**I. Feature visualization of the RGB-domain branch in the fourth layer of the encoder. The dotted box represents the constrained area of *Cross-Modal Loss*.**



(a) Constraint at the beginning of training (b) Constraint at the middle of training  
**II. Comparison of strategies for adding *Edge Loss* to training.**

**Figure 10: Ablation experiments of Constraint Strategy.**

**4.4.2 Effectiveness of the Depth Guidance Fusion Module.** Comparing with the Baseline roughly employed the concatenation operation between two modalities, we show the ablation results of the *Depth Guidance Fusion Module* in Fig8. From Fig8(c), it only transits in the blurred area for the position of the structural level

difference shown by the sparse depth, especially for foreground objects that are different from the background depth. In contrast, our module could highlight establishing different layers of depth distribution in the Fig8(d), as far as possible to restore the structure of the existence of depth, so that different objects and backgrounds can be easily distinguished. In Table3, the performance of our module has been significantly improved in crucial FID and AP scores.

**4.4.3 Effectiveness of Loss Design.** On the *Edge Loss* ablation, from the comparison in Fig7 and Fig9, the foreground object with edge constraint emphasizes contour accuracy. It weakens the blurred caused by the overlap. Additionally, we compare the training strategy about when to employ the *Edge Loss*. In Fig10II(a), the premature constraint before the model has built distinguishable content would lead to results in disordered performance.

And on the other *Cross-modal Loss* ablation, it achieves the optimal scores in Table3 and has more integrity of contour. It is more consistent than the previous results in semantic representation in Fig7. When choosing which layer to introduce the constraint, we adopt the middle layer (the fourth layer) in the encoder for implementation instead of the interaction carried out at the last layer features in previous studies. It is reasonable that the unknown area in the fourth layer has not established strong content, and the improvement obtained by increasing constraints is more evident and effective like Fig10I. The table 3 also shows that it gets a better improvement in score.

## 5 CONCLUSION

In this paper, we explore a novel reliable image outputting task combining sparse depth modality and propose the *Depth-Guided Outputting Network* to learn the structure-aware multimodal fusion. We explicitly rely on the differences and unique characteristics of the two modalities to design the *Multimodal Learning Module* and the *Depth Guidance Fusion Module* is designed to realize a progressive cross-modal fusion scheme to facilitate the extrapolated establishment. Furthermore, we design the additional *Cross-modal Loss* and *Edge Loss* to enhance the reliability of the results. The vehicle detection and comprehensive experiments demonstrate that our method enables image outputting with realistic and believable performance.

## REFERENCES

- [1] Coloma Ballester, Marcelo Bertalmio, Vicent Caselles, Guillermo Sapiro, and Joan Verdera. 2001. Filling-in by joint interpolation of vector fields and gray levels. *IEEE transactions on image processing* 10, 8 (2001), 1200–1211.
- [2] Connelly Barnes, Eli Shechtman, Adam Finkelstein, and Dan B Goldman. 2009. PatchMatch: A randomized correspondence algorithm for structural image editing. *ACM Trans. Graph.* 28, 3 (2009), 24.
- [3] Marcelo Bertalmio, Guillermo Sapiro, Vincent Caselles, and Coloma Ballester. 2000. Image inpainting. In *Proceedings of the 27th annual conference on Computer graphics and interactive techniques*. 417–424.
- [4] Richard Strong Bowen, Huiwen Chang, Charles Herrmann, Piotr Teterwak, Ce Liu, and Ramin Zabih. 2021. Oconet: Image extrapolation by object completion. In *Proceedings of the IEEE/CVF Conference on Computer Vision and Pattern Recognition*. 2307–2317.
- [5] John Canny. 1986. A computational approach to edge detection. *IEEE Transactions on pattern analysis and machine intelligence* 6 (1986), 679–698.
- [6] Djork-Arné Clevert, Thomas Unterthiner, and Sepp Hochreiter. 2015. Fast and accurate deep network learning by exponential linear units (elus). *arXiv preprint arXiv:1511.07289* (2015).
- [7] Dongsheng Guo, Hongzhi Liu, Haoru Zhao, Yunhao Cheng, Qingwei Song, Zhaorui Gu, Haiyong Zheng, and Bing Zheng. 2020. Spiral generative network



- for image extrapolation. In *European Conference on Computer Vision*. Springer, 701–717.
- [8] Kaiming He, Jian Sun, and Xiaoou Tang. 2010. Guided image filtering. In *European conference on computer vision*. Springer, 1–14.
  - [9] Martin Heusel, Hubert Ramsauer, Thomas Unterthiner, Bernhard Nessler, and Sepp Hochreiter. 2017. Gans trained by a two time-scale update rule converge to a local nash equilibrium. *Advances in neural information processing systems* 30 (2017).
  - [10] Mu Hu, Shuling Wang, Bin Li, Shiyu Ning, Li Fan, and Xiaojin Gong. 2021. Penet: Towards precise and efficient image guided depth completion. In *2021 IEEE International Conference on Robotics and Automation (ICRA)*. IEEE, 13656–13662.
  - [11] Sangwon Hwang, Junhyeop Lee, Woo Jin Kim, Sungmin Woo, Kyungjae Lee, and Sangyoun Lee. 2021. LiDAR Depth Completion Using Color-Embedded Information via Knowledge Distillation. *IEEE Transactions on Intelligent Transportation Systems* (2021).
  - [12] Bholeshwar Khurana, Soumya Ranjan Dash, Abhishek Bhatia, Aniruddha Mahapatra, Hrituraj Singh, and Kuldeep Kulkarni. 2021. SemIE: Semantically-aware Image Extrapolation. In *Proceedings of the IEEE/CVF International Conference on Computer Vision*. 14900–14909.
  - [13] Kyunghun Kim, Yeohun Yun, Keon-Woo Kang, Kyeongbo Kong, Siyeong Lee, and Suk-Ju Kang. 2021. Painting outside as inside: Edge guided image outpainting via bidirectional rearrangement with progressive step learning. In *Proceedings of the IEEE/CVF Winter Conference on Applications of Computer Vision*. 2122–2130.
  - [14] Diederik P Kingma and Jimmy Ba. 2014. Adam: A method for stochastic optimization. *arXiv preprint arXiv:1412.6980* (2014).
  - [15] Johannes Kopf, Wolf Kienzle, Steven Drucker, and Sing Bing Kang. 2012. Quality prediction for image completion. *ACM Transactions on Graphics (ToG)* 31, 6 (2012), 1–8.
  - [16] Kang Liao, Chunyu Lin, Yunchao Wei, Feng Li, Shangrong Yang, and Yao Zhao. 2021. Towards Complete Scene and Regular Shape for Distortion Rectification by Curve-Aware Extrapolation. In *Proceedings of the IEEE/CVF International Conference on Computer Vision*. 14569–14578.
  - [17] Guilin Liu, Fitsum A Reda, Kevin J Shih, Ting-Chun Wang, Andrew Tao, and Bryan Catanzaro. 2018. Image inpainting for irregular holes using partial convolutions. In *Proceedings of the European conference on computer vision (ECCV)*. 85–100.
  - [18] Lina Liu, Xibin Song, Xiaoyang Lyu, Junwei Diao, Mengmeng Wang, Yong Liu, and Liangjun Zhang. 2020. FCFR-Net: Feature fusion based coarse-to-fine residual learning for depth completion. *arXiv preprint arXiv:2012.08270* (2020).
  - [19] Takeru Miyato, Toshiki Kataoka, Masanori Koyama, and Yuichi Yoshida. 2018. Spectral normalization for generative adversarial networks. *arXiv preprint arXiv:1802.05957* (2018).
  - [20] Takeru Miyato and Masanori Koyama. 2018. cGANs with projection discriminator. *arXiv preprint arXiv:1802.05637* (2018).
  - [21] Deepak Pathak, Philipp Krahenbuhl, Jeff Donahue, Trevor Darrell, and Alexei A Efros. 2016. Context encoders: Feature learning by inpainting. In *Proceedings of the IEEE conference on computer vision and pattern recognition*. 2536–2544.
  - [22] Olaf Ronneberger, Philipp Fischer, and Thomas Brox. 2015. U-net: Convolutional networks for biomedical image segmentation. In *International Conference on Medical image computing and computer-assisted intervention*. Springer, 234–241.
  - [23] Josef Sivic, Biliiana Kaneva, Antonio Torralba, Shai Avidan, and William T Freeman. 2008. Creating and exploring a large photorealistic virtual space. In *2008 IEEE Computer Society Conference on Computer Vision and Pattern Recognition Workshops*. IEEE, 1–8.
  - [24] Christian Szegedy, Vincent Vanhoucke, Sergey Ioffe, Jon Shlens, and Zbigniew Wojna. 2016. Rethinking the inception architecture for computer vision. In *Proceedings of the IEEE conference on computer vision and pattern recognition*. 2818–2826.
  - [25] Jie Tang, Fei-Peng Tian, Wei Feng, Jian Li, and Ping Tan. 2020. Learning guided convolutional network for depth completion. *IEEE Transactions on Image Processing* 30 (2020), 1116–1129.
  - [26] Piotr Teterwak, Aaron Sarna, Dilip Krishnan, Aaron Maschinot, David Belanger, Ce Liu, and William T Freeman. 2019. Boundless: Generative adversarial networks for image extension. In *Proceedings of the IEEE/CVF International Conference on Computer Vision*. 10521–10530.
  - [27] Jonas Uhrig, Nick Schneider, Lukas Schneider, Uwe Franke, Thomas Brox, and Andreas Geiger. 2017. Sparsity Invariant CNNs. In *International Conference on 3D Vision (3DV)*.
  - [28] Dmitry Ulyanov, Andrea Vedaldi, and Victor Lempitsky. 2017. Improved texture networks: Maximizing quality and diversity in feed-forward stylization and texture synthesis. In *Proceedings of the IEEE conference on computer vision and pattern recognition*. 6924–6932.
  - [29] Miao Wang, Yu-Kun Lai, Yuan Liang, Ralph R Martin, and Shi-Min Hu. 2014. Biggerpicture: data-driven image extrapolation using graph matching. *ACM Transactions on Graphics* 33, 6 (2014).
  - [30] Yi Wang, Xin Tao, Xiaoyong Shen, and Jiaya Jia. 2019. Wide-context semantic image extrapolation. In *Proceedings of the IEEE/CVF Conference on Computer Vision and Pattern Recognition*. 1399–1408.
  - [31] Yaxiong Wang, Yunchao Wei, Xueming Qian, Li Zhu, and Yi Yang. 2021. Sketch-guided scenery image outpainting. *IEEE Transactions on Image Processing* 30 (2021), 2643–2655.
  - [32] Chaohao Xie, Shaohui Liu, Chao Li, Ming-Ming Cheng, Wangmeng Zuo, Xiao Liu, Shilei Wen, and Errui Ding. 2019. Image inpainting with learnable bidirectional attention maps. In *Proceedings of the IEEE/CVF International Conference on Computer Vision*. 8858–8867.
  - [33] Yan Xu, Xinge Zhu, Jianping Shi, Guofeng Zhang, Hujun Bao, and Hongsheng Li. 2019. Depth completion from sparse lidar data with depth-normal constraints. In *Proceedings of the IEEE/CVF International Conference on Computer Vision*. 2811–2820.
  - [34] Zongxin Yang, Jian Dong, Ping Liu, Yi Yang, and Shuicheng Yan. 2019. Very long natural scenery image prediction by outpainting. In *Proceedings of the IEEE/CVF International Conference on Computer Vision*. 10561–10570.
  - [35] Raymond A Yeh, Chen Chen, Teck Yian Lim, Alexander G Schwing, Mark Hasegawa-Johnson, and Minh N Do. 2017. Semantic image inpainting with deep generative models. In *Proceedings of the IEEE conference on computer vision and pattern recognition*. 5485–5493.
  - [36] Jiahui Yu, Zhe Lin, Jimei Yang, Xiaohui Shen, Xin Lu, and Thomas S Huang. 2018. Generative image inpainting with contextual attention. In *Proceedings of the IEEE conference on computer vision and pattern recognition*. 5505–5514.
  - [37] Jiahui Yu, Zhe Lin, Jimei Yang, Xiaohui Shen, Xin Lu, and Thomas S Huang. 2019. Free-form image inpainting with gated convolution. In *Proceedings of the IEEE/CVF International Conference on Computer Vision*. 4471–4480.
  - [38] Lingzhi Zhang, Jiancong Wang, and Jianbo Shi. 2020. Multimodal image outpainting with regularized normalized diversification. In *Proceedings of the IEEE/CVF Winter Conference on Applications of Computer Vision*. 3433–3442.
  - [39] Richard Zhang, Phillip Isola, Alexei A Efros, Eli Shechtman, and Oliver Wang. 2018. The unreasonable effectiveness of deep features as a perceptual metric. In *Proceedings of the IEEE conference on computer vision and pattern recognition*. 586–595.
  - [40] Xiaofeng Zhang, Feng Chen, Cailing Wang, Ming Tao, and Guo-Ping Jiang. 2020. Sienet: Siamese expansion network for image extrapolation. *IEEE Signal Processing Letters* 27 (2020), 1590–1594.
  - [41] Yinda Zhang, Jianxiong Xiao, James Hays, and Ping Tan. 2013. Framebreak: Dramatic image extrapolation by guided shift-maps. In *Proceedings of the IEEE Conference on Computer Vision and Pattern Recognition*. 1171–1178.
  - [42] Laurent Zwald and Sophie Lambert-Lacroix. 2012. The berhu penalty and the grouped effect. *arXiv preprint arXiv:1207.6868* (2012).